Conf-9106285--2

CMU-HEP--91-12

DE92 002771

RECENT RESULTS ON CHARM DECAYS AT $\sqrt{s} \approx 10$ GEV *

Michael Procario
Department of Physics
Carnegie Mellon University
Pittsburgh, Pennsylvania 15213
(representing the CLEO collaboration)

Abstract

Recent results on decays of charm particles are presented. The CLEO collaboration has measured two body decay modes of D_s involving η, η' or ρ^+, using the new CLEO II detector. They also have new measurements of the branching ratios of the D^{*0} and D^{*+}. In charm baryon decays, results from CLEO II are presented for $\Lambda_c^+ \to \Sigma^0\pi^+$, $\Lambda_c^+ \to \Lambda\pi^+\pi^0$, and the W-exchange process $\Xi_c^0 \to \Omega^- K^+$ has been observed in the CLEO I data.

*Talk presented at XI International Conference on Physics in Collision, Colmar, France June 20-22, 1991.

1 Introduction

The CLEO II detector has been accumulating data since late 1989 on or near the Υ resonances. The detector was designed for excellent reconstruction of both charged and neutral particles. The detector consists of a charged particle tracking system, surrounded by a time-of-flight system and an electromagnetic calorimeter consisting of 7800 CsI crystals. The Cornell Electron Storage Ring (CESR) has also been upgraded. The luminosity now routinely reaches 1.8×10^{32} cm^2/s , and as much as 11 pb^{-1}have been accumulated in one day. This has produced some very large samples of charm particles for the newly improved detector to study.

2 D_s decay modes

The D_s was first observed in the $\phi\pi^+$ decay mode,[1] and many other hadronic modes have since been found,[2] however a significant fraction of D_s decays has not yet been accounted for. This lead to speculation that some large two-body decay modes might exist. There are two possibly large modes $D_s \to \eta\pi^+$ and $D_s \to \eta'\pi^+$ known, but the current measurements by different experiments are inconsistent. CLEO has new preliminary measurements of these two decay modes, and preliminary measurements of the previously unseen modes $\eta\rho^+$ and $\eta'\rho^+$, as well as confirmation of the mode $\phi\rho^+$.

The dataset used for all D_s decay studies was comprised of 689 pb^{-1}of data taken at the $\Upsilon(3S)$, $\Upsilon(4S)$ and at center-of-mass energies just above and below the $\Upsilon(4S)$. Photons were always required to have $|\cos\theta| < 0.7$, where θ is the angle with respect to the beam direction. In this region photons cross the minimum amount of material before entering the calorimeter. Each neutral energy cluster must have a least 30 MeV of energy and not match to a charged track projected into the calorimeter to be considered a photon. Charged tracks were required to have their measured ionization loss (dE/dx) within 2.5 standard deviations of the expected ionization loss for the particular hypothesis considered. In order to reduce combinatorial background, the momentum of the D_s was required to be above 3 GeV/c. To suppress background from $\Upsilon(3S)$ decays, which contain very little charm, it was required that the ratio of Fox-Wolfram moments, H_2/H_0,[3] be greater than 0.2 for events taken at the $\Upsilon(3S)$ energy. A low value of R_2 signifies a spherical event like the ggg decays from the $\Upsilon(3S)$, while a large value of R_2 signifies the jet-like structure that $q\bar{q}$ events have.

All modes are normalized to the mode $\phi\pi^+$. The ϕ candidates are selected by requiring that two oppositely charged tracks with dE/dx consistent with a kaon have a mass within ± 8 MeV of the known ϕ mass. Additional requirements based on the angular correlation of the D_s decay products are added to reduce background. Since the D_s is spin zero, the ϕ must be uniformly distributed in angle in the D_s rest frame. The background tends to be peaked in the direction of D_s in the lab, so we require the $\cos\alpha_\phi < 0.8$, where α_ϕ, which we call the decay angle, is the angle between the ϕ in the D_s rest frame and the direction of the D_s in the lab. Since the ϕ is polarized in a helicity zero state, the kaons have a $\cos^2\theta_{K^+}$ distribution, where θ_{K^+}, which

we call the helicity angle, is the angle between the K^+ and the D_s in the ϕ rest frame. We require $|\cos\theta_{K^+}| > 0.45$. We found 453 ± 28 D_s decays. The efficiency to reconstruct $D_s^+ \to \phi\pi^+$ is calculated by Monte Carlo simulation and is found to be 17%. Throughout this paper charge conjugate states are also included.

2.1 The decay modes $D_s^+ \to \eta\pi^+$, and $\eta\prime\pi^+$

The decay modes $\eta\pi^+$, and $\eta\prime\pi^+$ were first observed by MARK II, and they found them to be large.[4] searched for the η by its decays to $\gamma\gamma$ and $\pi^+\pi^-\pi^0$, for which the branching ratios are 38.9% and 23.6% respectively. The $\gamma\gamma$ mass distribution is given by the histogram in figure 1(a). The background is dominated by photons from π^0 decays. When photons that combine with another photon to form a π^0 with momentum greater than 0.8 GeV/c are eliminated, the $\gamma\gamma$ distribution is given by the square points in figure 1(a). Monte Carlo simulations predict that this procedure keeps 92% of the η's and reduces the background by 50%. The fitted η width is 14 MeV (r.m.s.).

In the $\pi^+\pi^-\pi^0$ decay mode, the π^0 candidates are required to have a $\gamma\gamma$ mass within 2.5 times the r.m.s. width of the known π^0 mass. The r.m.s. width is approximately 5 MeV/c^2 and slightly momentum dependent. For each π^0 candidate the momentum is found by a kinematic fit of the photon momenta, with the constraint that the $\gamma\gamma$ mass be the known π^0 mass. The π^0 momentum was required to be greater than 0.3 GeV/c to be used in a η candidate. The $\pi^+\pi^-\pi^0$ mass distribution is shown is figure 1(b). The fitted width of the η signal is 6.0 MeV/c^2. In both modes the figure shows only combinations with momentum greater than 1.5 GeV/c to most clearly display the signal, however this cut was not used in D_s search. used in the analysis

The $\eta\prime$ was detected in the decay modes $\pi^+\pi^-\eta$ and $\rho^0\gamma$, which have branching ratios of 44.2% and 30.0%. In the $\pi^+\pi^-\eta$ mode the η is required to have momentum greater than 0.3 GeV/c to suppress background. In the $\rho^0\gamma$ mode, the photon momentum must be greater than 0.1 GeV/c, and $500\ \mathrm{MeV}/c^2 < M_{\pi^+\pi^-} < 850\ \mathrm{MeV}/c^2$, since the shape of the ρ^0 is distorted by limited phase space. The ρ^0 is polarized, so to optimize signal background we require $|\cos\theta_\pi^+| < 0.8$, where θ_π^+ is the angle between the π^+ direction and the photon direction in the ρ^0 rest frame. The mass plots for the $\eta\prime$ are shown in figure 2, where the $\eta\prime$ momentum is greater than 1.5 GeV/c. In figure 2(a) shows only the $\pi^+\pi^-\eta$ mode, and 2(b) shows the $\rho^0\gamma$ mode, which is large but on a large background, due to the width of the ρ^0. It is however quite significant. As in the η case, no minimum momentum was required of the $\eta\prime$ in the D_s search.

Figure 3 shows the $\eta\pi^+$ invariant mass distribution for both η decay modes. In the $\pi^+\pi^-\pi^0$ decay mode of the η, the π^0 was required to have a momentum greater than 0.3 GeV/c to reduce background from slow π^0's. The invariant mass spectrum was fitted in two ways. The first used gaussians of the Monte Carlo predicted width at the D_s and D^+ masses, a polynomial background function and the Monte Carlo predicted shape of $\eta\pi^+$ from $D_s^+ \to \eta\rho^+$. The second did not used the shape from the $\eta\rho^+$ reflection, but excluded the region where it occurred from the fit. The two fits agree within 5%. The efficiencies are found by Monte Carlo simulation. The results

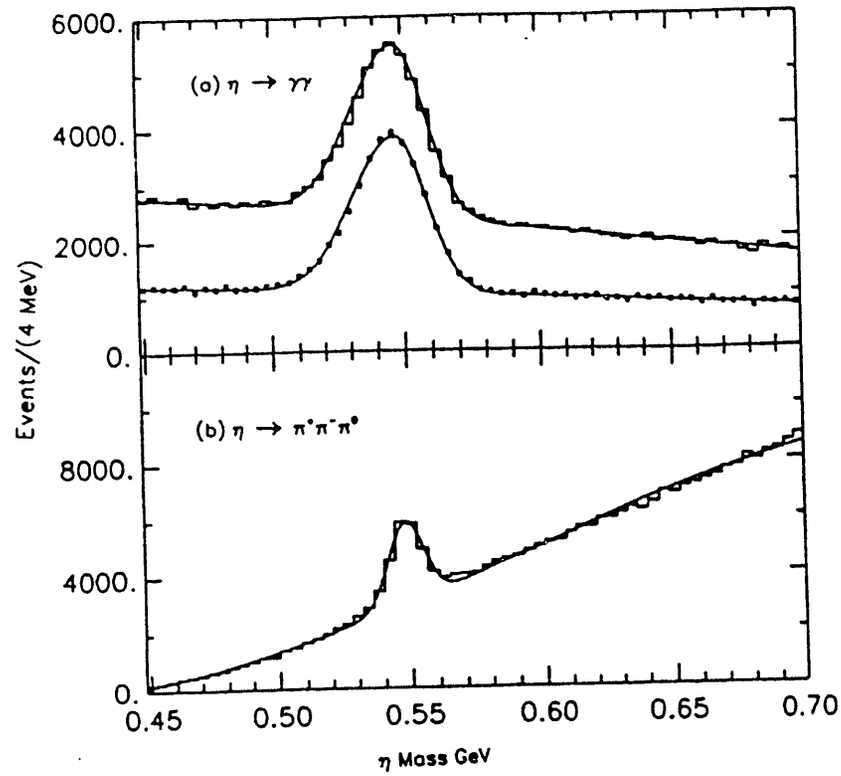

Figure 1: a) The $\gamma\gamma$ mass distributions for $p > 1.5$GeV/c histogram all combinations and square points after π^0 veto. b) The $\pi^+\pi^-\pi^0$ mass distribution for $p > 1.5$GeV/c.

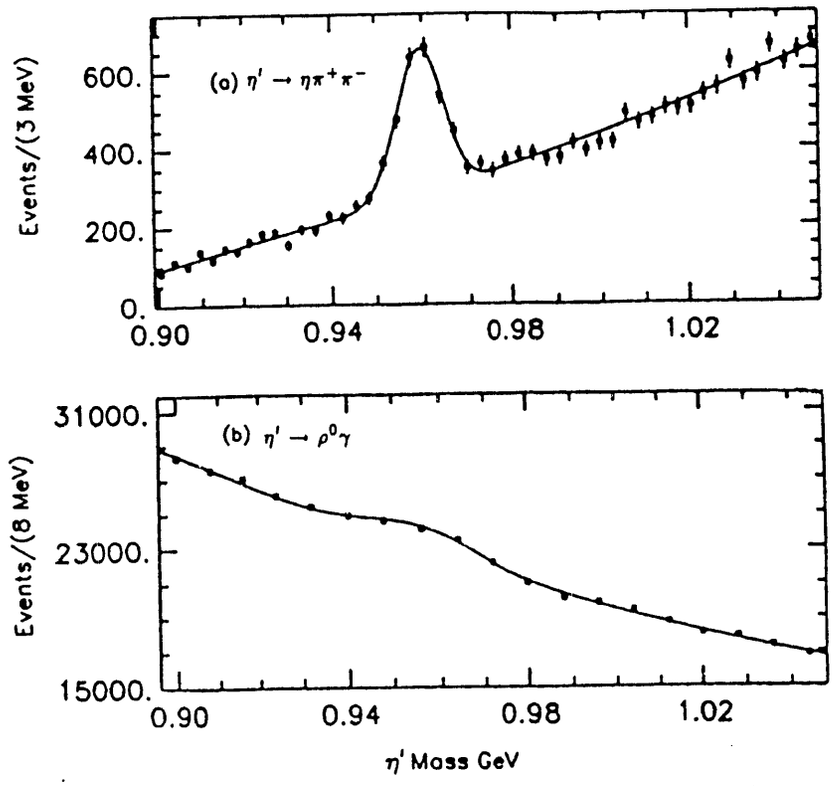

Figure 2: a) The $\pi^+\pi^-\eta$ mass distributions for $p > 1.5$GeV/c b) The $\rho^0\gamma$ mass distribution for $p > 1.5$GeV/c.

Mode	$s\bar{s}$ mode	number of events	efficiency (%)	$\Gamma/\Gamma(\phi\pi^+)$
$\phi\pi^+$	$\phi \to K^+K^-$	453 ± 28	17.0	1.0
$\eta\pi^+$	$\eta \to \gamma\gamma$	123 ± 24	8.17	0.56 ± 0.11 ± 0.10
$\eta\pi^+$	$\eta \to \pi^+\pi^-\pi^0$	42 ± 12	3.14	0.49 ± 0.15 ± 0.07
$\eta'\pi^+$	$\eta' \to \eta\pi^+\pi^-$ $\eta \to \gamma\gamma$	59 ± 11	2.05	1.10 ± 0.21 ± 0.17
$\eta'\pi^+$	$\eta' \to \eta\pi^+\pi^-$ $\eta \to \pi^+\pi^-\pi^0$	22 ± 7	0.75	1.12 ± 0.36 ± 0.17
$\eta'\pi^+$	$\eta' \to \rho^0\gamma$	200 ± 34	5.40	1.38 ± 0.25 ± 0.20

Table 1: Relative branching fractions for π^+ modes

for each individual decay mode can be found in table 1. When both decay modes are averaged, we find $\Gamma(D_s^+ \to \eta\pi^+)/\Gamma(D_s^+ \to \phi\pi^+) = 0.54 \pm 0.09 \pm 0.09$, where the first uncertainty is statistical and the second systematic.

Figure 4 shows the $\eta'\pi^+$ invariant mass distribution for both η' decay modes. The background shape was studied similarly to the $\eta\pi^+$ case, and once again the systematic uncertainty attributed to the background shape was 5%. The event yields, efficiencies and relative decay widths of all distinct final states are given in table 1. Averaging over all three different η' decay modes, we find $\Gamma(D_s^+ \to \eta'\pi^+)/\Gamma(D_s^+ \to \phi\pi^+) = 1.20 \pm 0.15 \pm 0.18$.

Our results for these two modes are compared with other measurements from E691,[5] Mark II,[4] Mark III,[6] NA14/2,[7] and ARGUS,[8], which can be seen in table 2. We obtain values that are consistent all upper limits, much smaller than Mark II, and just barely consistent with ARGUS and NA14/2. From our measurements one would conclude that $\eta\pi^+$ and $\eta'\pi^+$ are not major contributors to the total decay width of the D_s .

2.2 The decay modes $D_s^+ \to \eta\rho^+, \eta'\rho^+$, and $\phi\rho^+$

The small branching ratios for $\eta\pi^+$, and $\eta'\pi^+$ decay modes mean those modes cannot account for a significant fraction of the total D_s hadronic decay width. The CLEO II detector's excellent electromagnetic calorimeter makes it possible to also search for modes involving $\rho^+ \to \pi^+\pi^0$. Only the mode $D_s \to \phi\pi^+\pi^0$ has been seen previously, and the small statistics made it impossible to determine whether this mode comes from $\phi\rho^+$.[5]

The $\eta\pi^+\pi^0$ mass spectrum is shown in figure 5, for the case where the η decay to $\gamma\gamma$. The mass of the $\pi^+\pi^0$ combination was required to lie with ±170 MeV of the

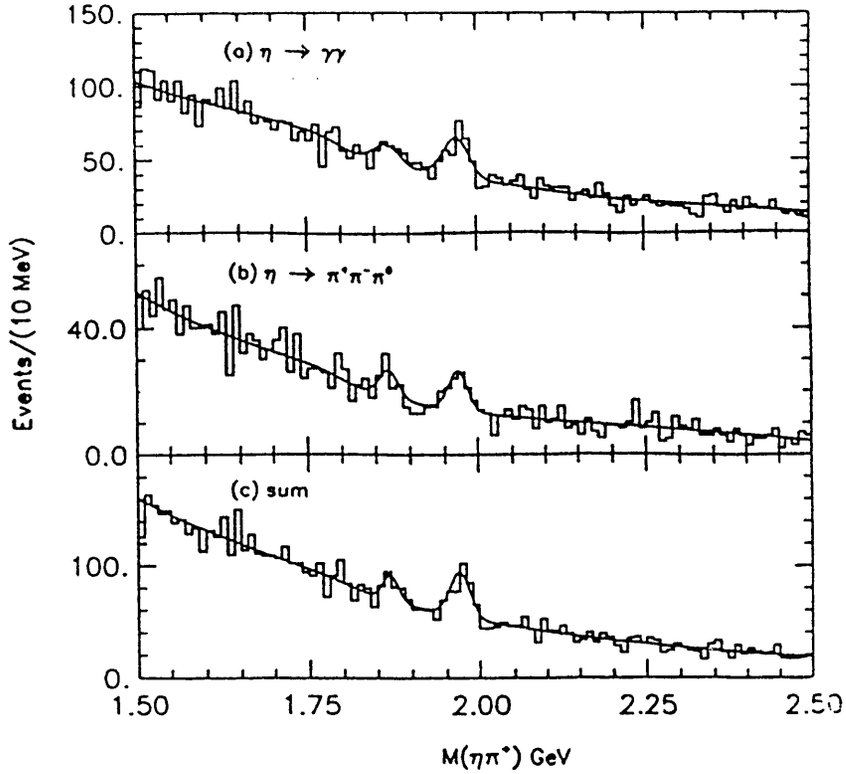

Figure 3: The $\eta\pi^+$ invariant mass spectrum using (a) the $\eta \to \gamma\gamma$ decay mode, (b) the $\eta \to \pi^+\pi^-\pi^0$ decay mode, and (c) the sum of the two modes.

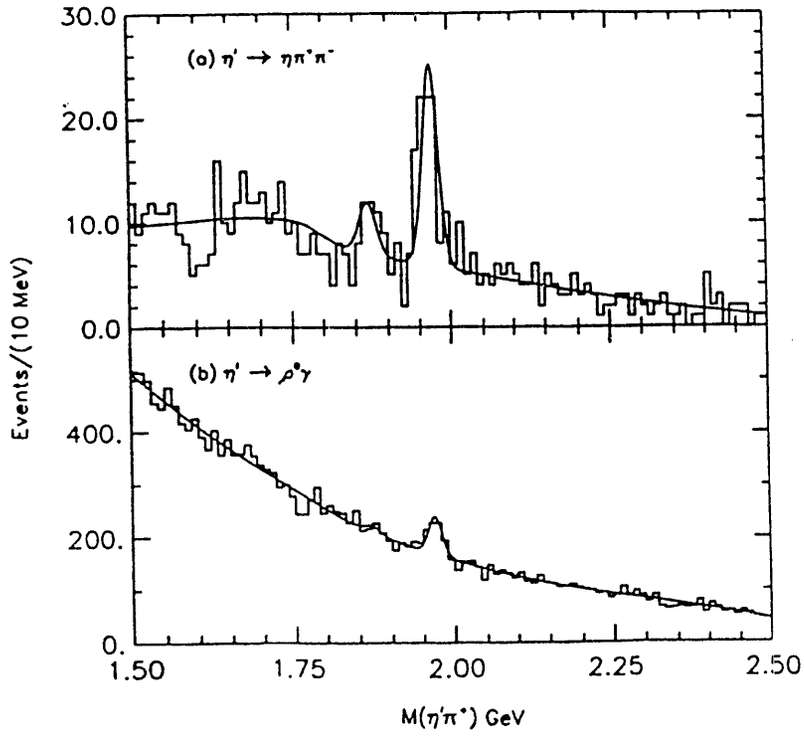

Figure 4: The $\eta\prime\pi^+$ invariant mass spectrum using (a) the $\eta\prime \to \pi^+\pi^-\eta$ decay mode, for the $\eta \to \gamma\gamma$ case (b) the $\eta\prime \to \rho^0\gamma$ decay mode.

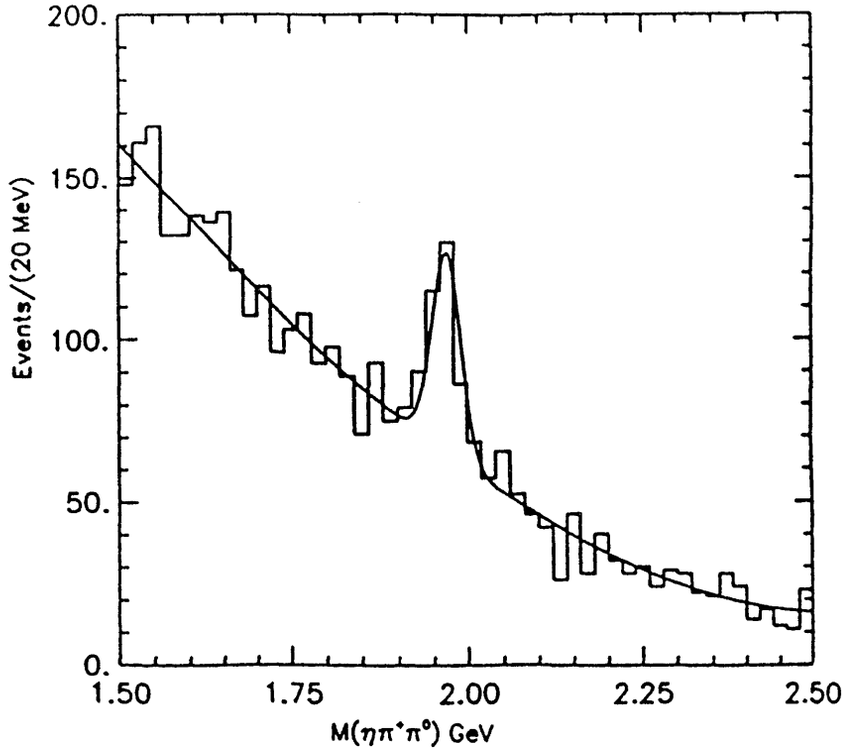

Figure 5: The $\eta\pi^+\pi^0$ invariant mass spectrum when the η decays to $\gamma\gamma$. The $\pi^+\pi^0$ mass must be within ± 170 MeV/c^2 of the ρ^+ mass.

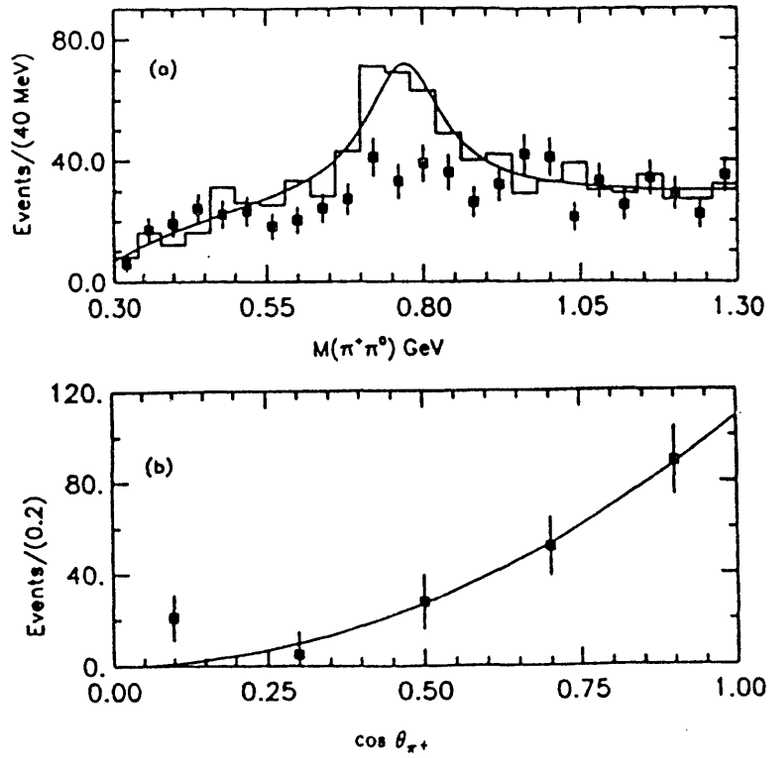

Figure 6: a) The $\pi^+\pi^0$ invariant mass spectrum for events in the D_s peak for the $\eta\pi^+\pi^0$ channel (histogram) and sidebands (solid points). b) The number of D_s events as a function of helicity angle, $\theta_{\pi+}$. The curve is a fit to $\cos^2\theta_{\pi+}$.

Experiment	$\Gamma(\eta\pi^+)/\Gamma(\phi\pi^+)$	$\Gamma(\eta'\pi^+)/\Gamma(\phi\pi^+)$
CLEO II	$0.54 \pm 0.09 \pm 0.09$	$1.20 \pm 0.15 \pm 0.18$
E691	< 1.5 @ 90% c.l.	< 1.3 @ 90% c.l.
Mark II	4.0 ± 1.3	6.4 ± 2.8
Mark III	< 2.5 @ 90% c.l.	< 1.9 @ 90% c.l.
NA14/2		$2.5 \pm 1.0^{+1.5}_{-0.4}$
ARGUS		2.5 ± 0.7

Table 2: Comparison of experimental results for D_s to $\eta\pi^+$ and $\eta'\pi^+$

ρ^+ mass. There were helicity angle and decay angle cuts on the π^+ and ρ^+ identical to those on the K^+ and ϕ in the $\phi\pi^+$ mode. There is a peak of 158 ± 22 at the D_s mass. Two test were performed to see if this peak was due to ρ^+ or uncorrelated $\pi^+\pi^0$. The first test released the mass cut on the $\pi^+\pi^0$ combinations and plotted the the $\pi^+\pi^0$ mass spectrum for $\eta\pi^+\pi^0$ combinations at the D_s mass and in the D_s sidebands. Figure 6(a) shows that the combinations from the D_s peak (histogram) have an enhancement at the ρ^+, while the sidebands (solid points) do not. The second test released the helicity angle cut on the π^+ and the $\eta\pi^+\pi^0$ combinations were binned in the helicity angle θ_{π^+}. The number of D_s's in each bin was found by fitting the mass spectra. The number of events as function of θ_{π^+} is shown in figure 6(b). The curve is a fit to the expected $\cos^2$ distribution. The fit has a confidence level of 38%. The non-resonant background is estimated by the amount of isotropic contribution allowed in the fit, and is at most 20%. A similar analysis was performed when the η decayed to $\pi^+\pi^-\pi^0$. The details of the number of events, efficiency and relative decay widths are given in table 3. The last asymmetric uncertainty on the relative decay widths reflects our estimate of how much of the $\pi^+\pi^0$ can be attributed to ρ^+. The average of the two η modes gives a branching ratio of $2.86 \pm 0.38 \pm 0.50^{+0.0}_{-0.57}$ times the branching ratio for the decay mode $\phi\pi^+$.

In the $\eta'\rho^+$ analysis, only the $\eta' \to \eta\pi^+\pi^-$ decay is used. When the $\eta' \to \rho^0\gamma$ mode is used the background in the $\eta'\pi^+\pi^0$ mass plot peaks near the D_s mass. In this final state, the maximum energy available to the $\pi^+\pi^0$ system is ≈ 1 GeV, and the limit of phase space is near the peak of the ρ^+. It complicates the extraction of a ρ^+ component from the $\pi^+\pi^0$ non-resonant component. The $\eta'\pi^+\pi^0$ mass spectrum is shown in figure 7, for the case where $\eta \to \gamma\gamma$. The $\pi^+\pi^0$ mass is required to be within ± 170 MeV/c^2, and the same decay angle and helicity angle cuts are made as the $\eta\rho^+$ case. The peak at the D_s contains 53 ± 10 events. The solid squares are combinations where the $\pi^+\pi^0$ mass is less than 500 MeV/c2. There is no sideband above the the ρ. No signal is visible in this lower sideband. We once again perform two tests to distinguish ρ^+ from $\pi^+\pi^0$. In figure 8(a) we show the $\pi^+\pi^0$ mass spectrum for events from the D_s peak (histogram) and from the D_s sidebands (solid points).

Mode	$s\bar{s}$ mode	number of events	efficiency (%)	$\Gamma/\Gamma(\phi\pi^+)$
$\eta\rho^+$	$\eta \to \gamma\gamma$	158 ± 22	2.02	$2.93 \pm 0.45 \pm 0.50^{+0.0}_{-0.59}$
$\eta\rho^+$	$\eta \to \pi^+\pi^-\pi^0$	59 ± 15	0.82	$2.70 \pm 0.68 \pm 0.50^{+0.0}_{-0.54}$
$\eta'\rho^+$	$\eta' \to \eta\pi^+\pi^-$ $\eta \to \gamma\gamma$	53 ± 10	0.56	$3.55 \pm 0.71 \pm 0.50^{+0.0}_{-0.71}$
$\eta'\rho^+$	$\eta' \to \eta\pi^+\pi^-$ $\eta \to \pi^+\pi^-\pi^0$	15 ± 6	0.18	$3.10 \pm 1.24 \pm 0.50^{+0.0}_{-0.62}$
$\phi\rho^+$	$\phi \to K^+K^-$	253 ± 32	5.10	$1.86 \pm 0.26 \pm 0.30^{+0.0}_{-0.56}$

Table 3: Relative branching fractions for ρ^+ modes

The is an enhancement at the ρ^+ only for the D_s signal region. In figure 8(b) we show the number of D_s events as a function of the helicity angle. The fit is to $\cos^2\theta_{\pi^+}$ and the confidence level is 10%. Again, the maximum possible contribution of non-resonant $\pi^+\pi^0$ is 20%. The details of this analysis and the analysis where $\eta \to \pi^+\pi^-\pi^0$ are given in table 3. The average branching ratio using both η decay modes is $3.44 \pm 0.62 \pm 0.52^{+0.0}_{-0.69}$.

The $\phi\pi^+\pi^0$ mass plot is the histogram in figure 9. The $\pi^+\pi^0$ invariant masses are required to be within ± 170 MeV/c^2 of the ρ^+ mass. A clear peak is seen with 253 ± 32 events. Testing whether the $\pi^+\pi^0$ are from a ρ^+ is harder than in the η and η' cases. The shape of the ρ^+ is even more distorted by phase space limitations than in the η' case, and the ρ^+ is not completely polarized as in the two previous cases. The dashed histogram in figure 9 shows the mass plot for $\phi\pi^+\pi^0$, where the $\pi^+\pi^0$ mass is below 500 MeV/c^2. No signal for the D_s is visible. The background in the mass plots reached its maximum near the D_s peak. we check that phase space or selection effects are not creating an artificial peak by plotting $\phi\pi^+\pi^-$ combinations with the mass of the $\pi^+\pi^-$ within ± 170 MeV/c^2 of the ρ^+ mass (solid points). This wrong sign background reasonably matches the background in $\phi\pi^+\pi^0$ and shows no evidence of a signal. We estimate a maximum of 30% non-resonant $\pi + \pi^0$ in the signal. The branching ratio for $D_s^+ \to \phi\rho^+$ is $1.86 \pm 0.26 \pm 0.30^{+0.0}_{-0.56}$ the branching ratio of $D_s^+ \to \phi\pi^+$.

The three D_s decay modes to $X\pi^+\pi^0$ are larger than $\phi\pi^+$ and in the η and η' cases there is good but not complete evidence than the $\pi^+\pi^0$ form a ρ^+. The evidence that ρ^+ dominates the $\phi\pi^+\pi^0$ channel is weaker but still there.

2.3 Comparison with theory

There are parameter-free predictions on the branching ratios for all of the above modes relative to $\phi\pi^+$ by Bauer, Stech and Wirbel.[9] For the $\eta\pi^+$ and $\eta'\pi^+$ results,

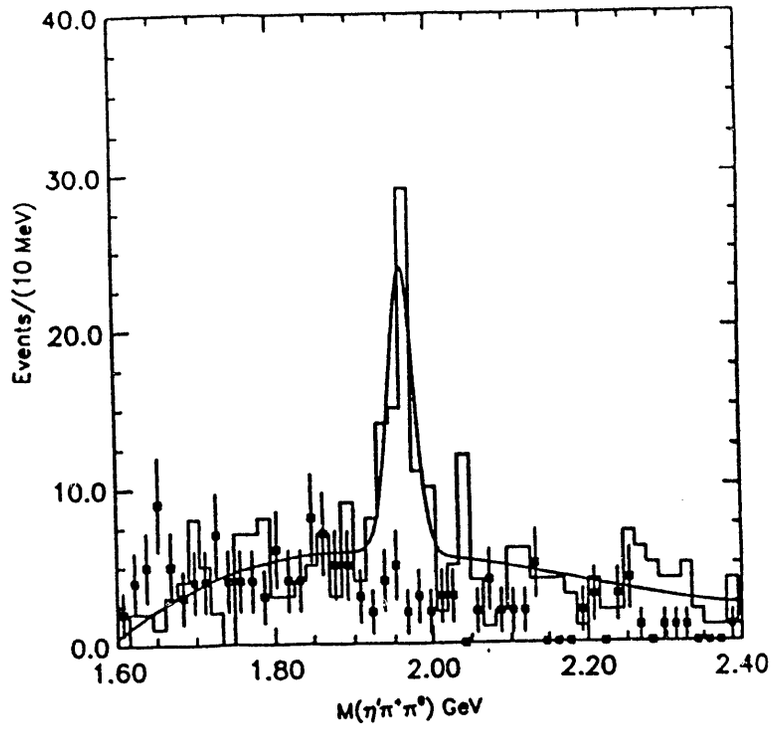

Figure 7: The $\eta\prime\pi^+\pi^0$ invariant mass spectrum when the η decays to $\gamma\gamma$. The $\pi^+\pi^0$ mass is within ± 170 MeV/c^2 of the ρ^+ mass for the histogram and $\pi^+\pi^0$ mass is below 500 MeV/c^2 for the solid points.

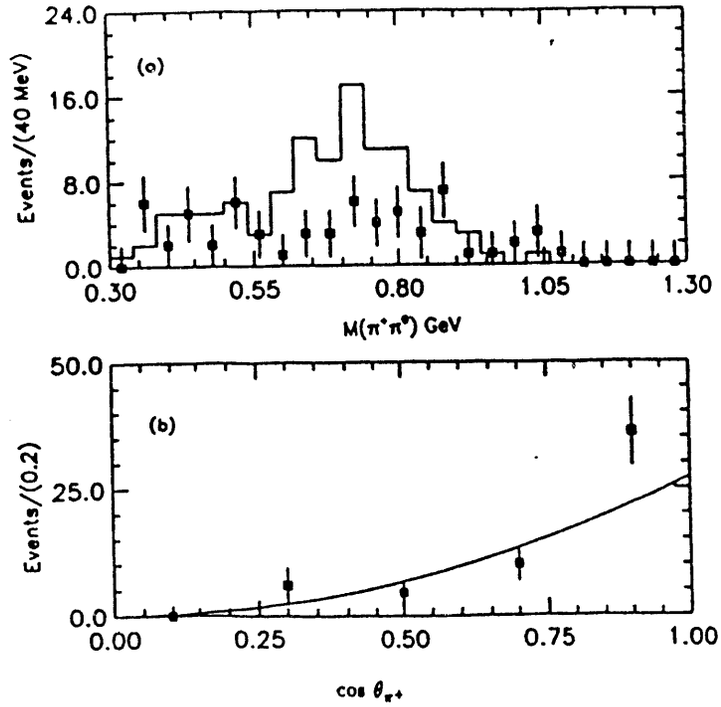

Figure 8: a) The $\pi^+\pi^0$ invariant mass spectrum for events in the D_s peak for the $\eta\prime\pi^+\pi^0$ channel (histogram) and sidebands (solid points). b) The number of D_s events as a function of helicity angle, θ_{π^+}. The curve is a fit to $\cos^2\theta_{\pi^+}$.

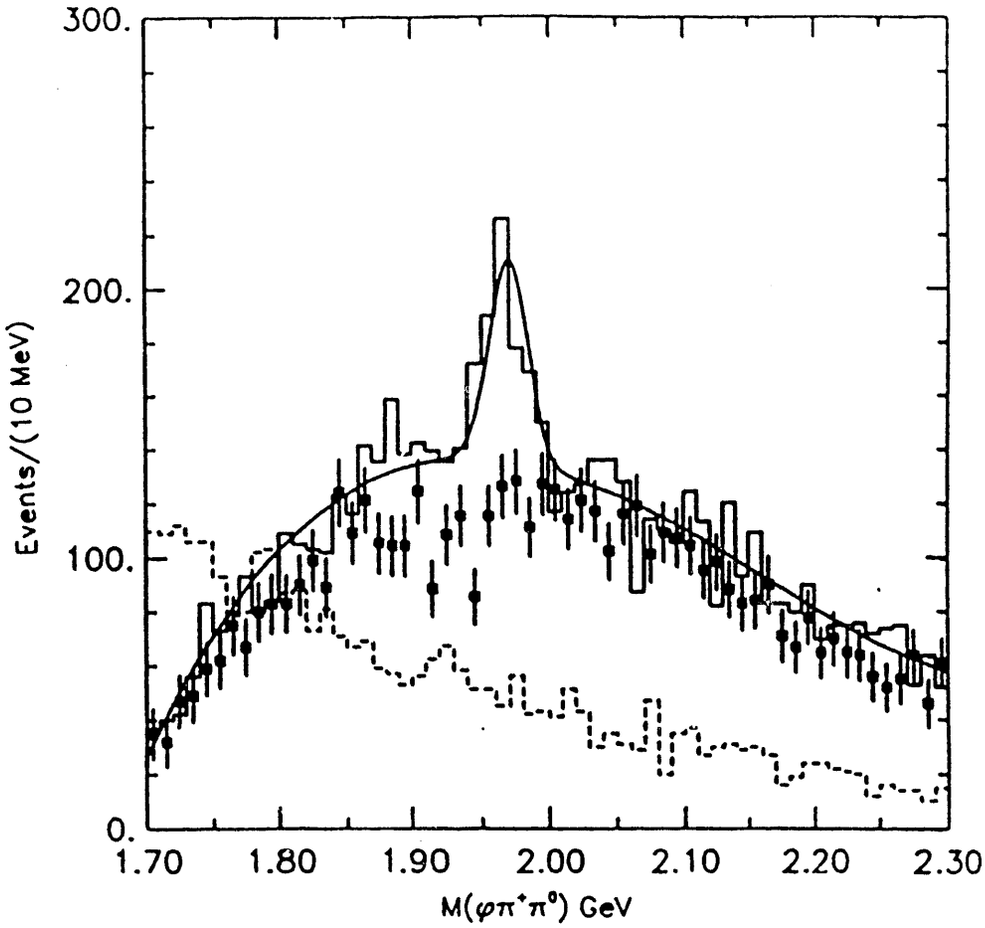

Figure 9: The $\phi\pi^+\pi^0$ invariant mass spectrum (histogram) for $\pi^+\pi^0$ invariant masses within ± 170 MeV/c^2 of the ρ^+ mass. The dashed line is for $\pi^+\pi^0$ invariant masses below 500 MeV/c^2, and the solid points are the invariant mass of $\phi\pi^\pm\pi^\mp$ combinations.

Kamal, Sinha and Sinha[10] have modified the BSW results by changing the $\eta - \eta'$C mixing angle. They also have made their own predictions. There are also predictions by Blok and Shifman.[12] The comparisons of theory and our measurements are given in table 4. Overall, they do not describe the data well.

2.4 Fraction of known D_s decays

In order to calculate the total fraction of D_s decays that have been observed, it is necessary to find the absolute branching fraction of D_s to $\phi\pi^+$. CLEO and ARGUS have both made recent efforts to set this scale more accurately than is currently known. CLEO measures the ratio of $\phi e^+\nu$ to $\phi\pi^+$ decays of the D_s , and uses the known branching ratio for $D^+ \to K^{*0}e^+\nu$ and the measured D_s^+ and D^+ lifetimes to predict what the value of $B(D_s^+ \to \phi e^+\nu)$ to set the absolute scale for $\phi\pi^+$. This technique requires a simple input from theory. Using an average of the ISGW[13] and WBS[14] models CLEO found $B(D_s^+ \to \phi e^+\nu) = 3.1 \pm 0.6^{+0.9}_{-0.6} \pm 0.6\%$[16]. A recent modification to the ISGW model has been reported by D.Scora,[15] which changes the

Mode	This experiment	BSW	BSW modified	KSS	BS
$\phi\pi^+$	1	1	1	1	1
$\eta\pi^+$	$0.54 \pm 0.09 \pm 0.09$	1.04	0.75	1.35	1.13
$\eta'\pi^+$	$1.20 \pm 0.15 \pm 0.18$	0.61	0.78	1.47	0.10
$\eta\rho^+$	$2.86 \pm 0.38 \pm 0.50^{+0.0}_{-0.57}$	1.96			
$\eta'\rho^+$	$3.44 \pm 0.62 \pm 0.50^{+0.0}_{-0.69}$	0.56			
$\phi\rho^+$	$1.86 \pm 0.26 \pm 0.30^{+0.0}_{-0.56}$	6.30			

Table 4: Comparison of theoretical predictions with our measurements

CLEO result to $B(D_s^+ \to \phi e^+\nu) = 3.5 \pm 1.2\%$.[17]

ARGUS takes a similar but not identical approach. They measure $B(D_s^- \to \phi e^-\overline{\nu})/B(D_s^- \to \phi\pi^-)$ and $B(D_s^- \to K^{*0}e^-\overline{\nu})/B(D^- \to K^+\pi^-\pi^-)$, which they relate through the WBS model to find $B(D_s^- \to \phi\pi^-) = 2.4 \pm 1.0\%$.[18]

In addition, ARGUS has tried to make a model independent measurement of $B(D_s^- \to \phi\pi^-)$ by partially reconstructing the decay $\overline{B}^0 \to D^{*+}D_s^{*-}$. First they fully reconstruct the $D_s^{*-} \to D_s^-\gamma, D_s^- \to \phi\pi^-$ and partially reconstruct the D^{*+} without observing the D^0 decay, then they partially reconstruct D_s^{*-} without observing the D_s^- and fully reconstruct D^{*+}. Requiring the the B branching ratio to be independent of how it was reconstructed allows them to extract $B(D_s^- \to \phi\pi^-) = 1.4 \pm 0.7 \pm 0.4\%$.[19]

Our knowledge of the absolute scale of the D_s branching ratios remains confused. I will use the recent CLEO result of 3.5% to calculate the sum of all known modes. The modes presented in this paper have a sum of decay widths 10.1 ± 1.3 times the width of $\phi\pi^+$. Other well-known mode, $\phi\pi^+$, $\overline{K}^0K^+$, $\overline{K}^{*+}K^0$, $\overline{K}^{*0}K^+$, non-resonant $K^+K^-\pi^+$, $\phi\pi^+\pi^-\pi^+$, $f_0(975)\pi^+$, and non-resonant $\pi^+\pi^-\pi^+$, have a sum of widths of 5.4 ± 0.4 times the width of $\phi\pi^+$. This gives 15.5 ± 1.4 times the absolute branching fraction for $\phi\pi^+$, $3.5 \pm 1.2\%$, which equals 54 ± 19 %.

Adding the two semileptonic decays which are almost equal to the D^+ semileptonic branching ratio of $8 \pm 1\%$, and the theoretical estimate for the leptonic decays $B(D_s^+ \to \tau^+\nu$ and $\mu^+\nu) = 5\%$, gives a grand total of $\sim (75 \pm 19)\%$. The uncertainty is dominated by the uncertainty on $B(D_s^- \to \phi\pi^-)$.

3 $D^*(2010)$ branching ratios

The D^* branching ratios have been measured before,[2] but the Particle Data Group's averages are dominated by the Mark III measurements.[20] MARK III found that $B(D^{*+} \to D^+\gamma) = (17 \pm 5 \pm 5)\%$. This value is too large to be naturally acomadated by theoretical models. For example, the model of Brekke and Rosner predicts that $B(D^{*+} \to D^+\gamma) \approx 3\%$.[21] A large anomalous magnetic moment for the charm

quark is needed to explain the large branching ratio. If there are problems with the measurement of the radiative decay of the D^{*+} and the correct value is closer to the theoretical prediction, then $B(D^{*+} \to D^0\pi^+)$ and $B(D^{*+} \to D^+\pi^0)$ must be larger since the three branching ratios were constrained to sum to 1. This will effect the measurements of B meson branching fractions involving D^{*+}'s.

As previously mentioned, there are only three allowed decay modes for the D^{*+} , and there are only two modes for the D^{*0} , $D^0\gamma$ and $D^0\pi^0$, since the mode $D^+\pi^-$ is kinematically forbidden. Therefore by using

$$B(D^{*0} \to D^0\gamma) + B(D^{*0} \to D^0\pi^0) = 1 \tag{1}$$

$$B(D^{*+} \to D^+\gamma) + B(D^{*+} \to D^+\pi^0) + B(D^{*+} \to D^0\pi^+) = 1, \tag{2}$$

and measuring the ratios

$$R^0_\gamma = \frac{B(D^{*0} \to D^0\gamma)}{B(D^{*0} \to D^0\pi^0)}, \tag{3}$$

$$R^+_\gamma = \frac{B(D^{*+} \to D^+\gamma)}{B(D^{*+} \to D^+\pi^0)}, \tag{4}$$

and either measuring or using isospin invariance to calculate the ratio

$$R^0_\pi = \frac{B(D^{*+} \to D^0\pi^+)}{B(D^{*+} \to D^+\pi^0)} \tag{5}$$

all the branching ratios can be found. The ratios R^0_γ and R^+_γ can be found by counting the number of $D^0\gamma$, $D^0\pi^0$, $D^+\gamma$, and $D^+\pi^0$, and calculating the relative efficiency of finding the γ or π^0. For the ratio R^+_π the efficiencies are not as simple to calculate and the uncertainties in $B(D^0 \to K^-\pi^+)$ and $B(D^+ \to K^-\pi^+\pi+)$ contribute to the uncertainty on ratio. This ratio however is given by isospin invariance and phase space differences to be $R^+_\pi = 2.19 \pm 0.17$, where this uncertainty is due mainly the uncertainty on the D^* - D mass difference but is still smaller than can be obtained by a direct measurement.

The same dataset was used for this analysis as for the D_s analysis. The same event, track, photon and π^0 selections were used. The same cut on R_2 for $\Upsilon(3S)$ events was used. The D^* candidates were required to have a minimum momentum of 2.5 GeV/c instead of the 3.0 GeV/c required of D_s candidates. The $D^0 \to K^-\pi^+$ decay mode was used to 4 reconstruct D^0's and the $D^+ \to K^-\pi^+\pi^+$ mode was used to reconstruct D^+'s. For D^0 decays the K^- is isotropically distributed in the D^0 rest frame, while the background in backward in decay angle. We required $\cos\theta_K > -0.9$.

Each D^0 and D^+ candidates is combined with each remaining γ, π^0, or π^+ to form D^{*0} and D^{*+} candidates. (The charge conjugate states are also done.) In the $D\gamma$ there is a large background due to soft photons moving opposite the direction of the D. To reduce this we require $\cos\theta_\gamma > 0$, where θ_γ is the decay angle relative to the D^*. We then calculate $\delta = M^* - M - Q$, where $M*$ is the mass of the D^* candidate,

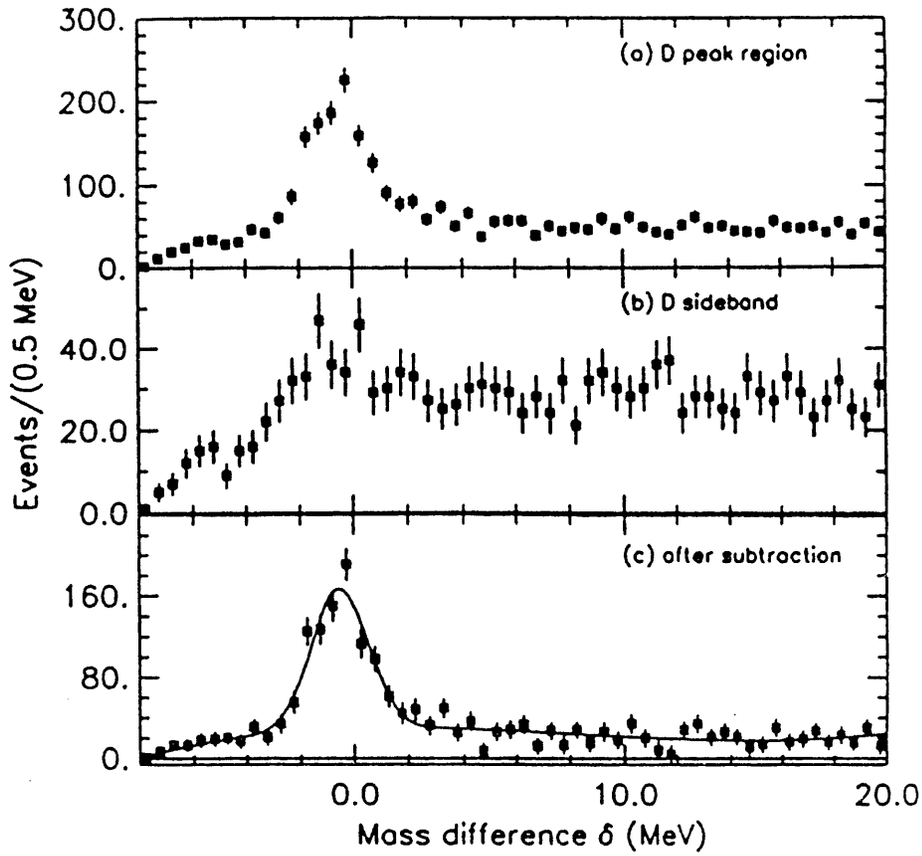

Figure 10: The mass difference, δ, distributions for $D^{*0} \rightarrow D^0\pi^0$. a) the D^0 peak region, b) the D^0 sideband region, c) difference of a and b.

M is the mass of the D candidate, and Q is the PDG[2] value of the $D^* - D$ mass difference.

In figure 10 the δ distributions can be seen for the decay $D^{*0} \rightarrow D^0\pi^0$. In figure 10(a) the delta distribution for events with the D^0 candidate with $\pm 2.5\sigma$ of the known D mass. A clear D^* signal is visible. In figure 10(b) the delta distribution for events with $1.790 < m_{K\pi} < 1.822$ GeV/c^2 and $1.908 < m_{K\pi} < 1.940$ GeV/c^2. These sidebands are expected to be good representations of the background under the D signal. A small signal is visible in the sideband plot. In figure 10(c) the signal and sideband distributions have been subtracted. This distribution is fitted to a gaussian signal and third-order polynomial background. The mean and width of the gaussian are determined by the fit. The mean value of δ found in the fit is -0.7 ± 0.4 MeV. The yield, mass difference resolution (both measured and expected from Monte Carlo), and reconstruction efficiency are given in table 5.

In figure 11 we show the δ distributions can be seen for the decay $D^{*0} \rightarrow D^0\gamma$. For $\delta < -50$ MeV, there is a large background from $D^{*0} \rightarrow D^0\gamma$ decays, where one of the γ's from the π^0 decay has been missed, but Monte Carlo calculations indicate that this background does not reach under the signal. The δ distribution is

Mode	Number of events	Mass Resolution Measured (MeV/c2)	Mass Resolution Monte Carlo (MeV/c2)	ϵ %
$D^{*0} \to D^0\gamma$	$557 \pm 71 \pm 40$	5.6 ± 0.4	5.2	15.7
$D^{*0} \to D^0\pi^0$	$724 \pm 56 \pm 26$	11.0 ± 0.05	1.16	15.4
$D^{*+} \to D^+\gamma$	$79 \pm 59 \pm 26$		5.2	13.5
$D^{*+} \to D^+\pi^0$	$629 \pm 37 \pm 25$	0.95 ± 0.07	1.17	13.3
$D^{*+} \to D^0\pi^+$	$2265 \pm 61 \pm 47$	0.80 ± 0.02	0.75	47.0

Table 5: The yields, mass difference resolutions both observed and expected and reconstruction efficiency by mode.

wider in this mode than the π^0 mode, because the momentum resolution of the π^0 is improved by kinematically fitting it. The mean value of δ is -0.12 ± 0.02. While this is statistically different from zero it also is an order of magnitude smaller than the uncertainty on the $D^* - D$ mass difference given by the PDG.[2] It should not be considered a measurement of the $D^* - D$ mass difference, since all systematic errors on the difference have not yet been studied. Once again the yields, mass resolutions and reconstruction efficiencies are given in table 5. Using the $n(D^0\gamma)$, $n(D^0\pi^0$ and the relative efficiency of finding a π^0 accompanying a D^0 to the efficiency of finding a γ accompanying a D^0, we find

$$R^0_\gamma = 0.75 \pm 0.11 \pm 0.13. \tag{6}$$

We can now calculate the ratio of D^{*0} branching ratios and using equation 1 find each branching ratio. The results are given in table 6 and are in good agreement with the current PDG[2] values.

In figure 12 we show the δ distributions for $D^{*+} \to D^+\gamma$. No peak is apparent in either the signal or sideband plots. The D^+ sidebands are defined to be $1.810 < m_{K\pi\pi} < 1.836$ GeV/c^2 and $1.913 < m_{K\pi\pi} < 1.939$ GeV/c^2. A fit to the unsubtracted δ distribution with a gaussian signal and third-order polynomial background yields $79 \pm 59 \pm 20$ events. The gaussian's mean was fixed at zero and its width was fixed to the measured width of the $D^0 \to D^0\gamma$ channel. The dashed line shows the expected signal for a 17% branching ratio.

A known background comes from $D_s^{*+} \to D_s^+\gamma$ decays, where the D_s^+ decays to $\phi\pi^+$ or $\overline{K}^{*0}K^+$, and one of the final state kaons is misinterpreted as a pion. If the $D^{*+} \to D^+\gamma$ events are reinterpreted as a D_s^{*+} we do observe small signals, and we estimate that as much as 40% of the $D^{*+} \to D^+\gamma$ could be D_s^{*+} background. At this stage we increase the systematic error from ± 20 to ± 40 events to account for this background. The yield with this error as well as resolution and efficiency for this mode are given in table 5.

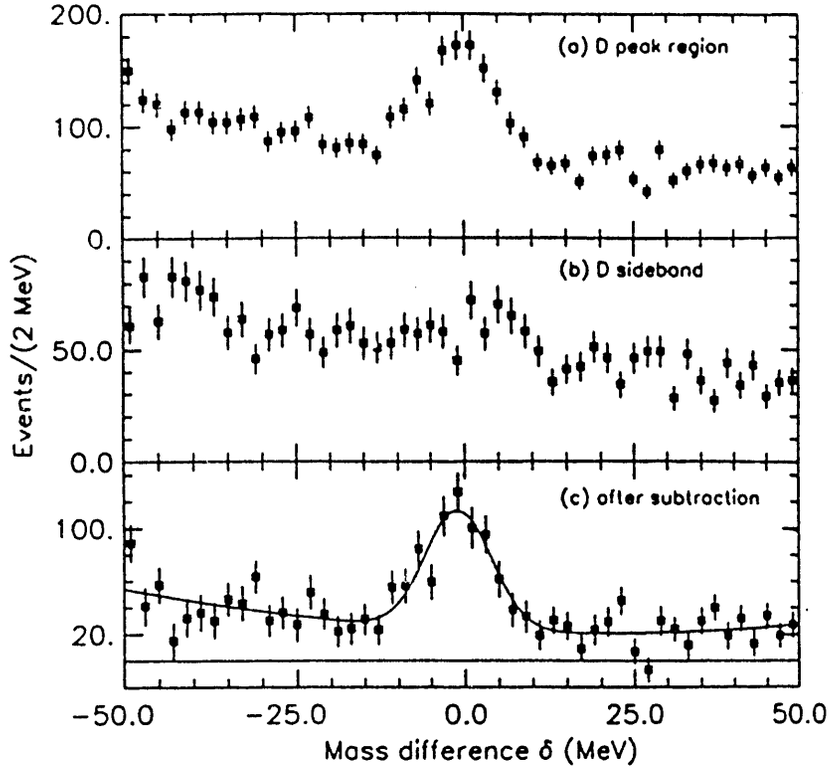

Figure 11: The mass difference, δ, distributions for $D^{*0} \rightarrow D^0\gamma$. a) the D peak region, b) the D sideband region, c) D peak region minus the sidebands

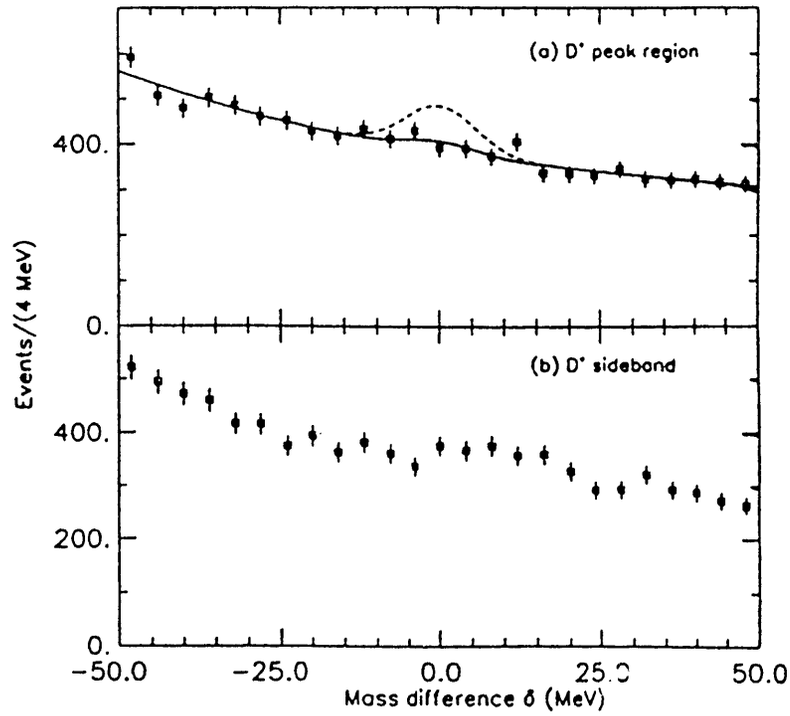

Figure 12: The mass difference, δ, distributions for $D^{*+} \rightarrow D^+\gamma$. a) the D^+ peak region, the dashed line is the signal expected for a 17% branching ratio b) the D^+ sideband region

Decay mode	Experimental ratio	With Isospin constraint	PDG value
$D^0 \to D^0\gamma$	$43.0 \pm 3.7 \pm 4.2$		45 ± 6
$D^0 \to D^0\pi^0$	$57.0 \pm 3.7 \pm 4.2$		55 ± 6
$D^+ \to D^+\gamma$	$3.8 \pm 2.8 \pm 2.0 \pm 2.0$	$3.7 \pm 2.7 \pm 1.9$	18 ± 4
$D^+ \to D^+\pi^0$	$30.9 \pm 1.6 \pm 4.4 \pm 4.4$	$30.2 \pm 0.8 \pm 1.6$	27.2 ± 2.5
$D^0 \to D^0\pi^+$	$65.3 \pm 2.4 \pm 5.1 \pm 5.1$	$66.1 \pm 1.8 \pm 2.2$	55 ± 4

Table 6: $D^*(2010)$ branching fractions. The D^{*+} modes are calculated two different ways. The first is with purely experimental input, and the second uses the isospin constraint to calculate R_π^+. The third error on the purely experimental values is due the uncertainty in the measured D^0 and D^+ branching ratios.

The data for $D^{*+} \to D^+\pi^0$ is shown in figure 13(a). There is no signal evident in the sideband data shown in figure 13(b), so we fit the unsubtracted distribution. The signal is fitted with a gaussian whose width comes from the fit, and the background is fitted by a function that simulates its threshold behaviour. The results of the fit are given in table 5. Just as in the D^{*0} case, we can find the ratio of branching ratios, which in this case give

$$R_\gamma^+ = 0.124 \pm 0.093 \pm 0.066. \tag{7}$$

Using the value of R_π^+ given by isospin, we can find all the D^{*+} branching ratios, which are displayed in the third column of table 6.

It is possible to check the previous result by measuring R_π^+. This requires $n(D^0\pi^+)$ and relative efficiency to reconstruct the two different final states. Figure 14(a) gives the δ distribution for $D^{*+} \to D^0\pi^+$ from the D^0 signal, and figure 14(b) shows the same distribution for the D^0 sidebands. Since there is a signal visible in the sideband δ distribution, we subtract it before fitting for $n(D^0\pi^+)$. The results are given in table 5. Using $\epsilon(D^+\pi^0)/\epsilon(D^0\pi^+) = 0.28 \pm 0.06$, we find

$$R_\pi^0 = 2.11 \pm 0.14 \pm 0.46 \pm 0.31, \tag{8}$$

where the last error is due to the uncertainty of the measured $D^0 \to K^-\pi^+$ and $D^+ \to K^-\pi^+\pi^+$ branching ratios. The D^{*+} branching ratios can now be found without the isospin constraint, and they are listed in table 6 column 2. The results using the isospin constraint and are in agreement not with the results that did not use it. We do not see a statistically significant signal for $D^{*+} \to D^+\gamma$ and we set the 90% confidence level upper limit of 8.0% on the branching ratio. This limit disagrees with the previous Mark III measurement, but is consistent with theoretical expectations.

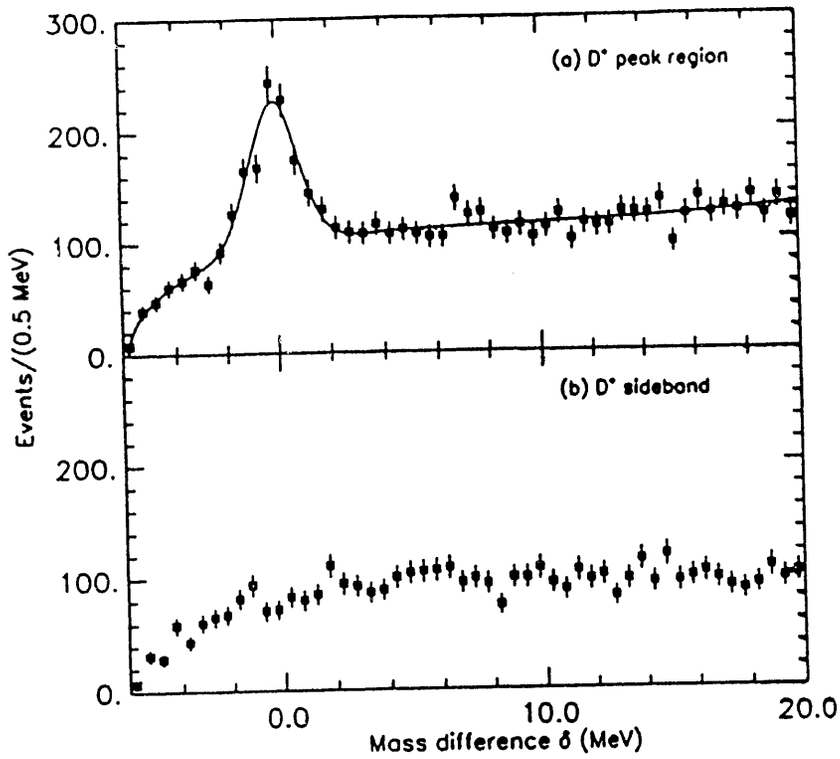

Figure 13: The mass difference, δ, distributions for $D^{*+} \rightarrow D^{+}\pi^{0}$. a) the D^{+} peak region, b) the D^{+} sideband region

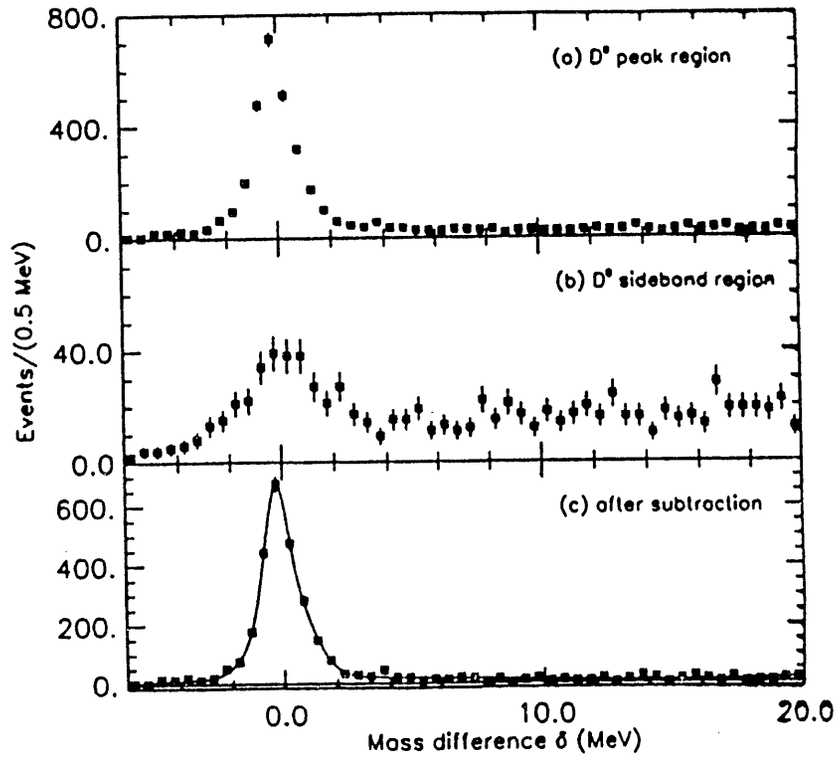

Figure 14: The mass difference, δ, distributions for $D^{*+} \rightarrow D^{0}\pi^{+}$. a) the D^{0} peak region, b) the D^{0} sideband region, c) D^{0} peak region minus the sidebands

4 Study of the Decays $\Lambda_c^+ \to \Sigma^0\pi^+$ and $\Lambda_c^+ \to \Lambda\pi^+\pi^0$

The Λ_c^+ was discovered over 15 years ago, and we can currently only account for 14% of its total branching fractions.[2] We know that its lifetime is shorter than the D^+, so decay mechanisms other than the spectator decay must be present. More detailed knowledge of the decay modes of the Λ_c^+ is needed to determine the existence and importance of these other mechanisms. We have measured the branching fraction for the mode $\Lambda_c^+ \to \Sigma^0\pi^+$, which had been previously observed in a bubble chamber experiment,[22] but there was no measurement of the branching fraction. We have also measured the branching ratio for the mode $\Lambda_c^+ \to \Lambda\pi^+\pi^0$, which has not been previously detected.

The dataset for this analysis consists of 879 $\text{pb}^{-1}$of data taken at the $\Upsilon(3S)$ resonance, as well as just below, just above and at the $\Upsilon(4S)$ resonance. Lambda candidates were reconstructed by pairing oppositely charged tracks and looking for a intersection away from the beam crossing point. The quality of the interaction was measured by a χ^2 value calculated from the distance between the tracks in the z direction and how well the momentum sum pointed back to the vertex. The higher momentum track was assumed to be the proton and was required to have a ionization energy loss measurement with 3.5 sigma of the expected ionization energy loss for a proton. We used lambda candidates with a mass within 2σ of the known lambda mass. Photons were always required to have $|\cos\theta| < 0.7$ and have energy greater than 30 MeV, as in the previous analyses. The energy in the 9 CsI crystals around the shower center had to have 90% of the energy in the 25 crystals around the shower center. This selection criterion prefers electromagnetic shower over hadronic showers. We also require that the photon candidate does not match to a charged track. Neutral pions are formed in a similar way as the previous analyses. The photon pairs within 10 MeV of the nominal π^0 mass and with greater than 250 MeV/c momentum are considered π^0 candidates.

We measure the Λ_c branching fractions relative to the decay mode $\Lambda\pi^+$. The $\Lambda\pi^+$ branching ratio has been measured relative to $B(\Lambda_c^+ \to pK^-\pi^+)$ by CLEO.[23] The systematic effects of lambda-finding efficiency and proton identification are the same in this mode and the two modes under study, so the systematic error is minimized by measuring the ratios of the decay rate to the mode $\Lambda\pi^+$. The mass distribution for the $\Lambda\pi^+$ decay mode is shown in figure 15. The shape below the peak is given by a Monte Carlo simulation of $\Lambda_c \to \Sigma^0\pi^+$, where the γ in the $\Sigma^0 \to \Lambda\gamma$ decay has not been observed. The area of this background was found in the fit to be 166 ± 19. The peak was fitted with a gaussian with its width fixed the Monte Carlo prediction of $\sigma = 23.9$ MeV. There are 166 ± 19 events in the peak. To check that the $\Sigma^0\pi^+$ background is restricted to only the region predicted by the Monte Carlo, we have examined the combinations with the wrong strangeness and charge, for example $\Lambda\pi^-$. This background is plotted with a dotted line in figure 15, and it agrees with the $\Lambda\pi^+$ background everywhere but the region populated by $\Sigma^0\pi^+$ background.

Σ^0 candidates were formed by combining lambdas with photons. Those lying within 2σ of the nominal Σ^0 mass were combined with charged pions. The mass

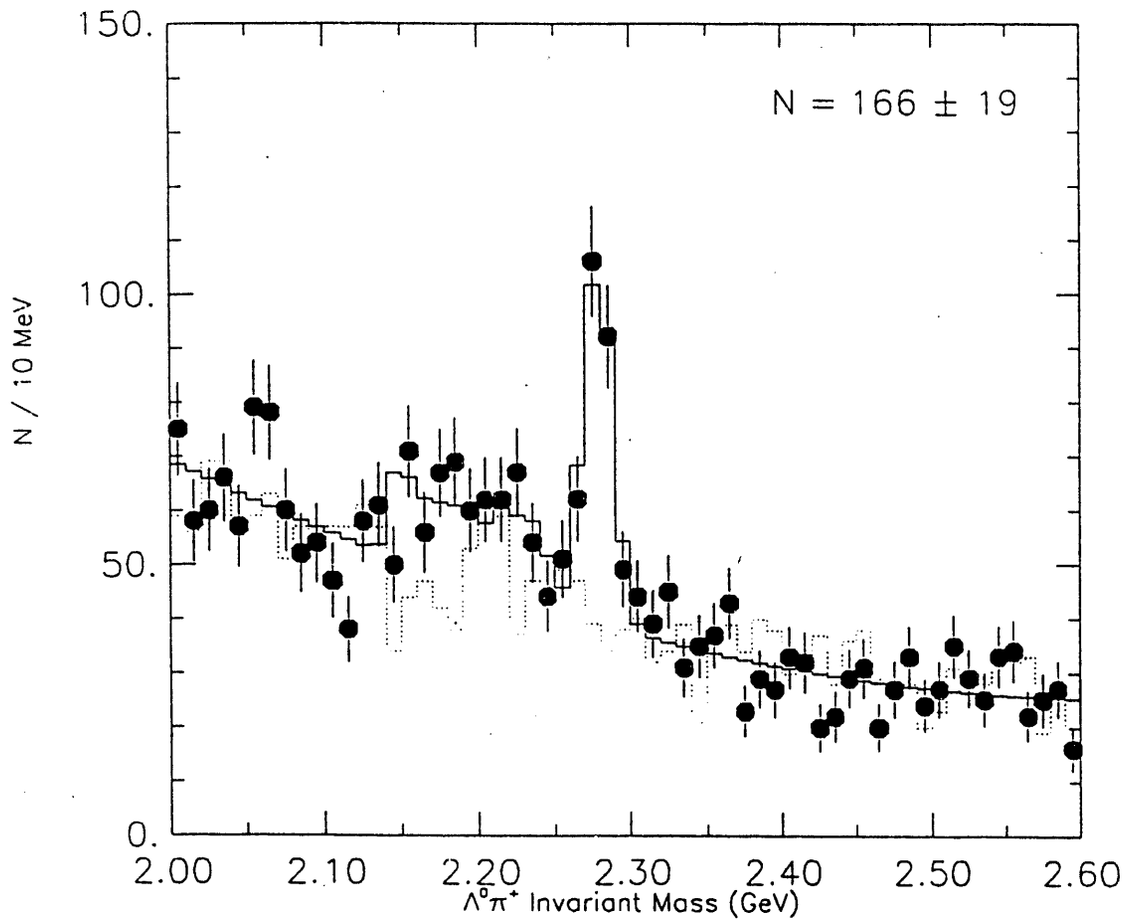

Figure 15: The $\Lambda\pi^+$ mass distribution. The background is fitted by a second order polynomial and a shape given by Monte Carlo for the decay $\Lambda_c \to \Sigma^0\pi^+$, where the γ in the $\Sigma^0 \to \Lambda\gamma$ decay has not been observed. The signal is fitted by gaussian with its width predicted by the Monte Carlo. The dotted line gives the wrong strangeness-charge combinations which should model backgrounds other than the $\Sigma^0\pi^+$ background.

distribution for $\Sigma^0\pi^+$ combinations is shown in figure 16. The mass distribution for $\Sigma^0\pi^+$ was fitted with a gaussian with its width fixed by the Monte Carlo to be $\sigma = 25.7$ MeV/c, and a second order polynomial. The number of events under the peak is 89 ± 13. The efficiency of finding an additional photon in an event with $\Lambda\pi^+$ is 51%. Therefore, the number of events expected in the background of the $\Lambda\pi^+$ mass distribution is 175 ± 25, which is in good agreement with what we found by fitting the $\Lambda\pi^+$ distribution. The result for the relative rate is

$$\frac{\Gamma(\Lambda_c^+ \to \Sigma^0\pi^+)}{\Gamma(\Lambda_c^+ \to \Lambda\pi^+)} = 1.0 \pm 0.2 \pm 0.1, \tag{9}$$

which is in disagreement with a recent theoretical prediction that the ratio is 5-to-1.[24]

Figure 17 shows the invariant mass distribution for $\Lambda\pi^+\pi^0$ combinations. The area under the gaussian with a fixed width of 33.2 MeV/c^2 is 91 ± 20 events. The

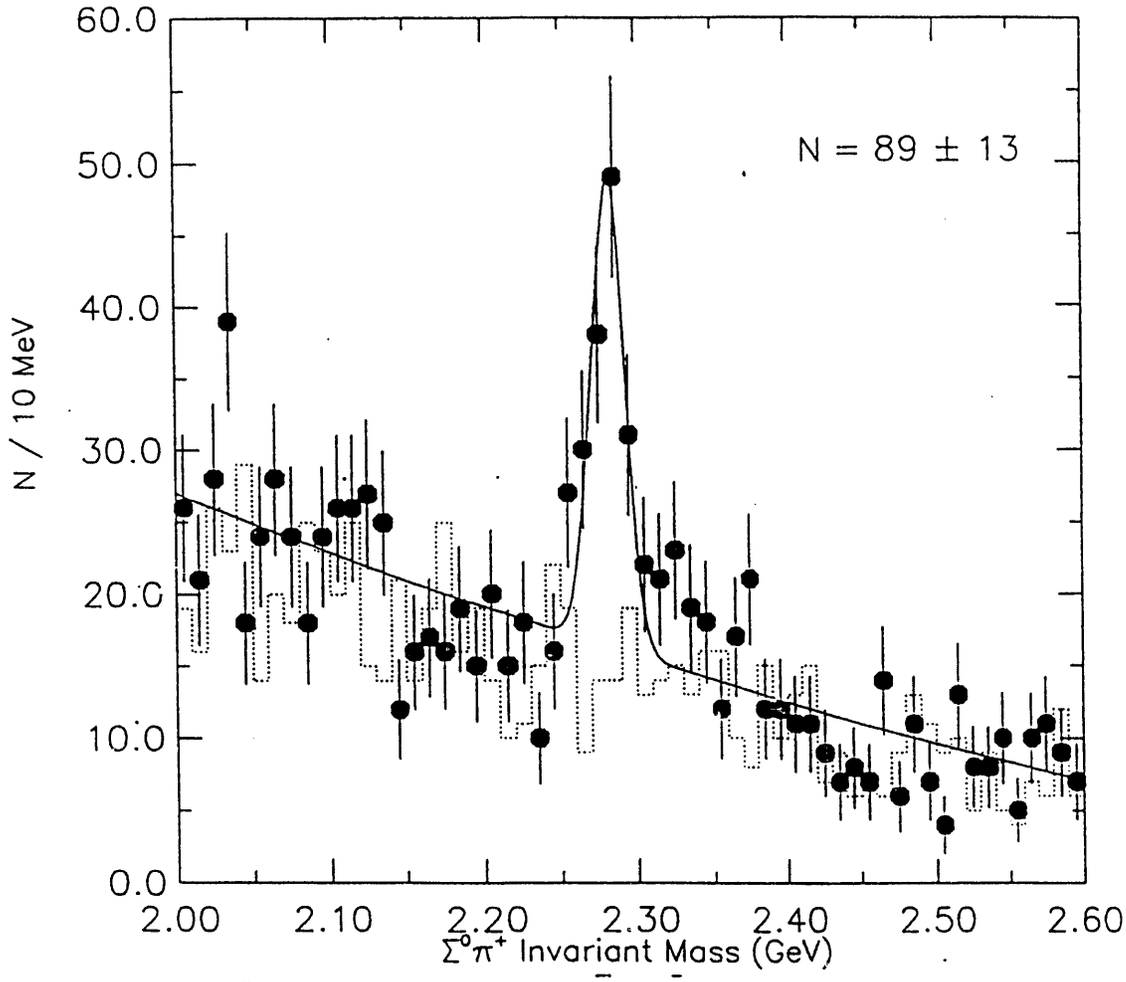

Figure 16: The $\Sigma^0\pi^+$ mass distribution. The background is fitted by a second order polynomial. The signal is fitted by gaussian with its width predicted by the Monte Carlo. The dotted line gives the wrong strangeness-charge combinations.

efficiency for detecting this channel was determined by Monte Carlo simulation, where the Λ_c decayed with a distribution given by three body phase space. The efficiency was found to be 20% of the efficiency for $\Lambda_c \to \Lambda\pi^+$, so the relative rate is,

$$\frac{\Gamma(\Lambda_c^+ \to \Lambda\pi^+\pi^0)}{\Gamma(\Lambda_c^+ \to \Lambda\pi^+)} = 2.7 \pm 0.8 \pm 0.5. \qquad (10)$$

We have not yet be able to determine the substructure of this decay.

5 Observation of the decay $\Xi_c^0 \to \Omega^- K^+$

The first signal for the Ξ_c^0 was found by CLEO[25] in the mode $\Xi_c^0 \to \Xi^-\pi^+$, and it has since been seen in the additional decay modes $\Xi_c^0 \to pK^-\overline{K}^{*0}$ by ACCMOR[26] and $\Xi_c^0 \to \Xi^-\pi^+\pi^-\pi^+$ARGUS[27]. We have now seen evidence for the new decay $\Xi_c^0 \to \Omega^- K^+$. While the previously observed modes can proceed by either internal or external spectator diagrams, this mode cannot. The most likely method is a W-exchange diagram, since W-exchange diagrams are not expected to be suppressed by

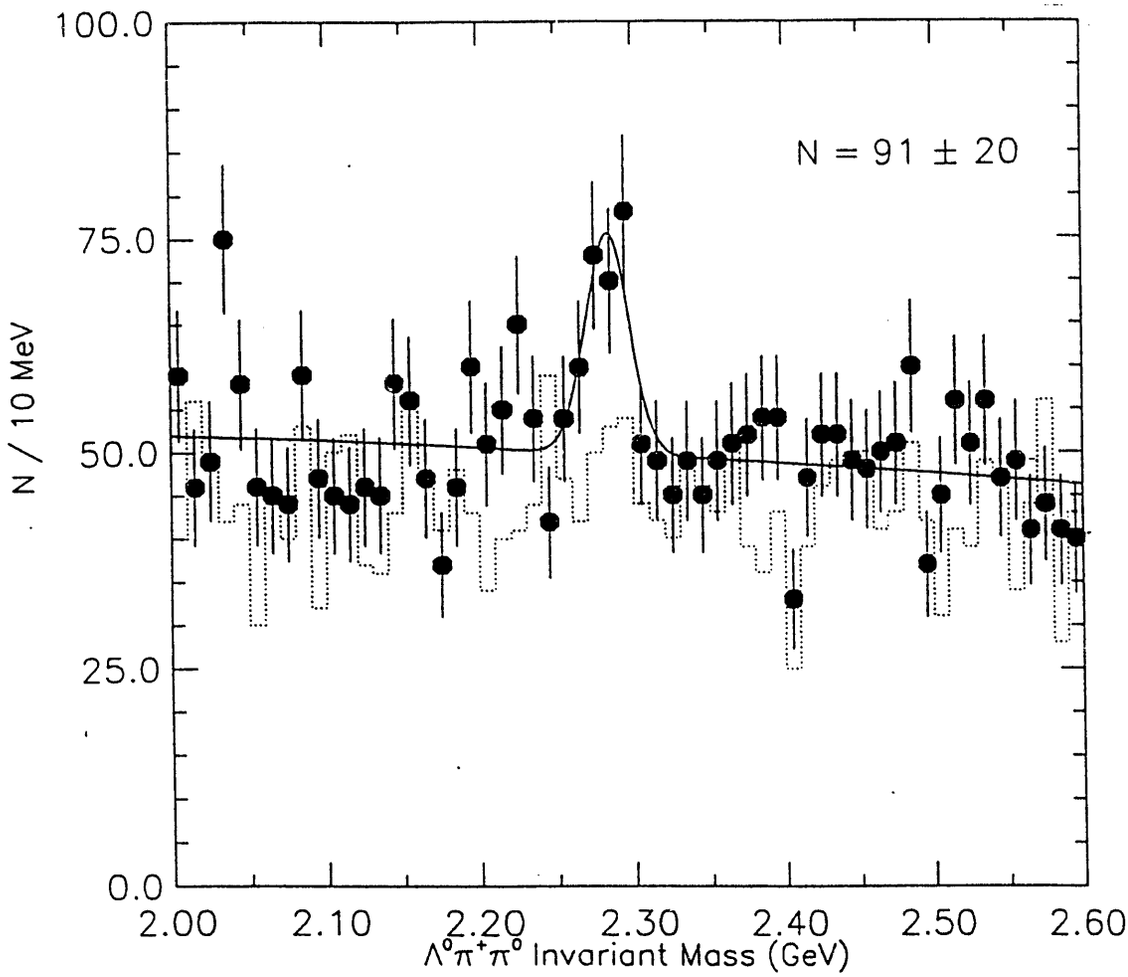

Figure 17: The $\Lambda\pi^+\pi^0$ mass distribution. The background is fitted by a second order polynomial. The signal is fitted by gaussian with its width predicted by the Monte Carlo. The dotted line gives the wrong strangeness-charge combinations.

helicity or colour conservation in charm baryon decays as they are in charm meson decays,[28] although final state interactions are very hard to rule out. The short lifetimes of Λ_c^+ and Ξ_c^0 could be explained if W-exchange diagrams are significant contributors to the total decay rate, however the only direct evidence up to now for W-exchange diagrams is some weak evidence for $\Delta^{++}K^-$ in the resonant substructure of $\Lambda_c^+ \to pK^-\pi^+$.[29]

This analysis was done on data taken with the CLEO detector, which is the predecessor of the CLEO II detector. It has been described elsewhere. [30] The dataset consists of 212 pb^{-1}taken at the $\Upsilon(4S)$, 106 pb^{-1}at the $\Upsilon(5S)$ and 101 pb^{-1}taken on the continuum just below the $\Upsilon(4S)$.

Ω^-'s are detected through the decay chain $\Omega^- \to \Lambda K^-$, $\Lambda \to p\pi^+$. Λ candidates are formed from oppositely charged tracks which intersect at a radial distance of more than 3 mm from the primary vertex. Unlike the Λ_c analysis, no requirement was made on how well the Λ pointed to the primary vertex, since they are produced away from the primary vertex at the Ω^- decay vertex. The proton candidate was required to have a dE/dx measurement within 3σ of that expected for a proton. The

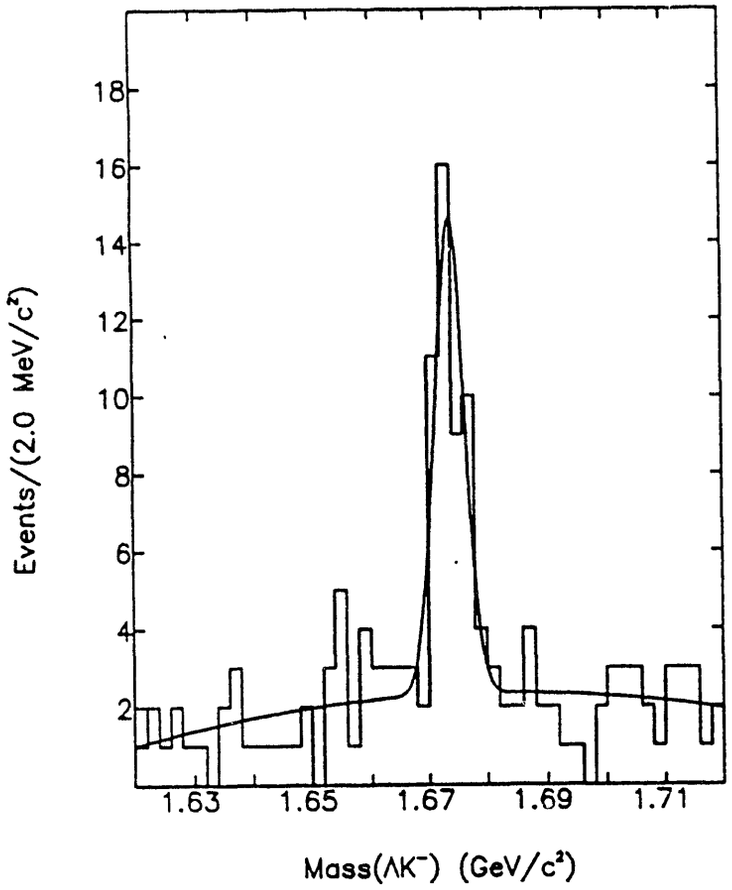

Figure 18: The ΛK^- mass distribution. The signal is fitted by gaussian with its width predicted by the Monte Carlo.

invariant mass of the $p\pi^+$ pair was required to be within 6 MeV/c^2 of the known Λ mass. Ω^- candidates were formed by combining Λ candidates with an additional negatively charged track with a dE/dx measurement within 2σ of that expected for a kaon. The point of intersection of the K^- and the Λ must be at least 3 mm from the primary vertex and closer to than the Λ vertex is. Both the Λ and the K^- were required to have impact parameters greater than 5 mm. This requirement prefers tracks from secondary vertices over tracks directly from the primary vertex. The ΛK^- mass distribution is shown in figure 18. The gaussian in the fit has its width fixed at the Monte Carlo predicted width of 6.0 MeV/c^2. The yield of Ω^-'s is 38 ± 8. The efficiency to detect an Ω^- was found by Monte Carlo to be a maximum of 11% at 2.5 GeV/c^2.

Those Ω^- candidates within 6 MeV/c^2 of the known Ω^- mass were combined with all K^+ candidates. The K^+ candidates were required to have a dE/dx measurement within 2σ of that expected for a kaon. The $\Omega^- K^+$ mass distribution is shown in figure 19. A fit to the distribution with a gaussian of fixed width and a flat background yields 8.5 ± 3.0 events and a mass of $2.469 \pm 0.002 \pm 0.003$ GeV/c^2, where the first uncertainty is statistical and the second is systematic. This value of the mass agrees

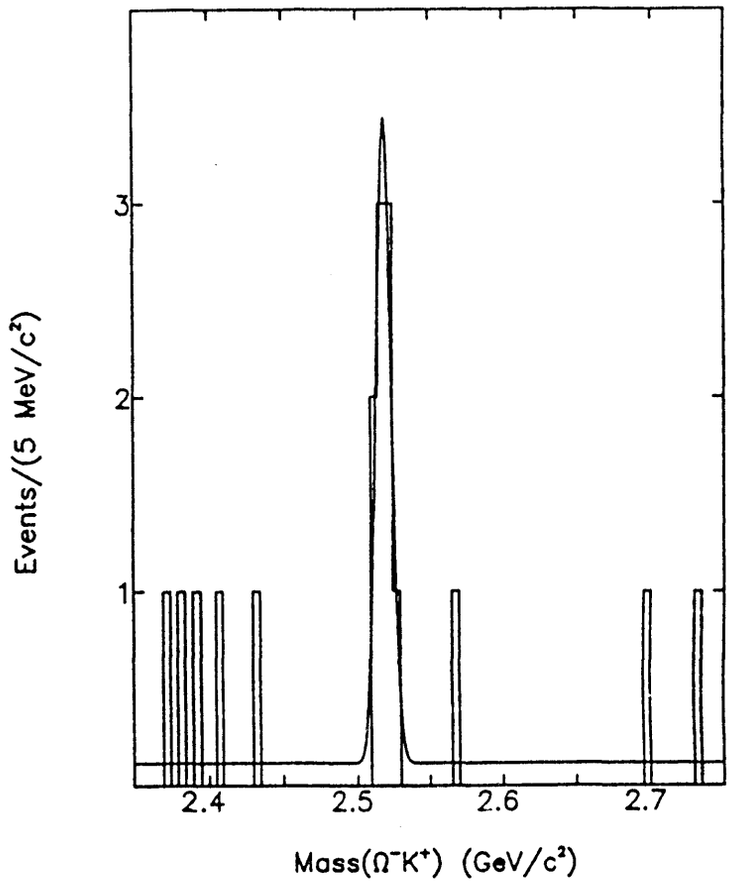

Figure 19: The ΩK^+ mass distribution. The signal is fitted by gaussian with its width predicted by the Monte Carlo. The background was assumed to be flat.

with our previous measurement in the mode $\Xi^-\pi^+$. If we define the Ξ_c^0 mass region to be $2.455\text{GeV}/c^2 < m_{\Lambda K} < 2.485\text{GeV}/c^2$, then there are 9 combinations where a flat background would predict 0.75 combinations.

We wish to compare our rate to the previously measured process $\Xi_c^0 \to \Xi^-\pi^+$, so we have reanalyzed[31] the decay $\Xi_c^0 \to \Xi^-\pi^+$ using the same vee-finder and no momentum cut. The Ξ^-'s were found from $\Lambda\pi^-$ combinations which intersected at least 5 mm from the primary vertex and have a mass with 6 MeV/c^2 of the Ξ^- mass. The mass distribution of $\Xi^-\pi^+$ combinations is given in figure 20. The yield of $\Xi_c^0 \to \Xi^-\pi^+$ decays is 38 ± 9. Monte Carlo simulations predict an efficiency of 12% for $\Xi^-\pi^+$, while it is 6% for ΩK^- averaged over the entire momentum range. The relative decay rates are given by

$$\frac{\Gamma(\Xi_c^0 \to \Omega K^-)}{\Gamma(\Xi_c^0 \to \Xi^-\pi^+)} = 0.50^{+0.21}_{-0.11}. \tag{11}$$

This result implies that 25 ± 10 % of all Ω^-'s produced in e^+e^- collisions are the results of a single decay channel. This only seems possible if Ω_c production is small compared to Ξ_c^0 production, since the Ω_c is expected to decay frequently to

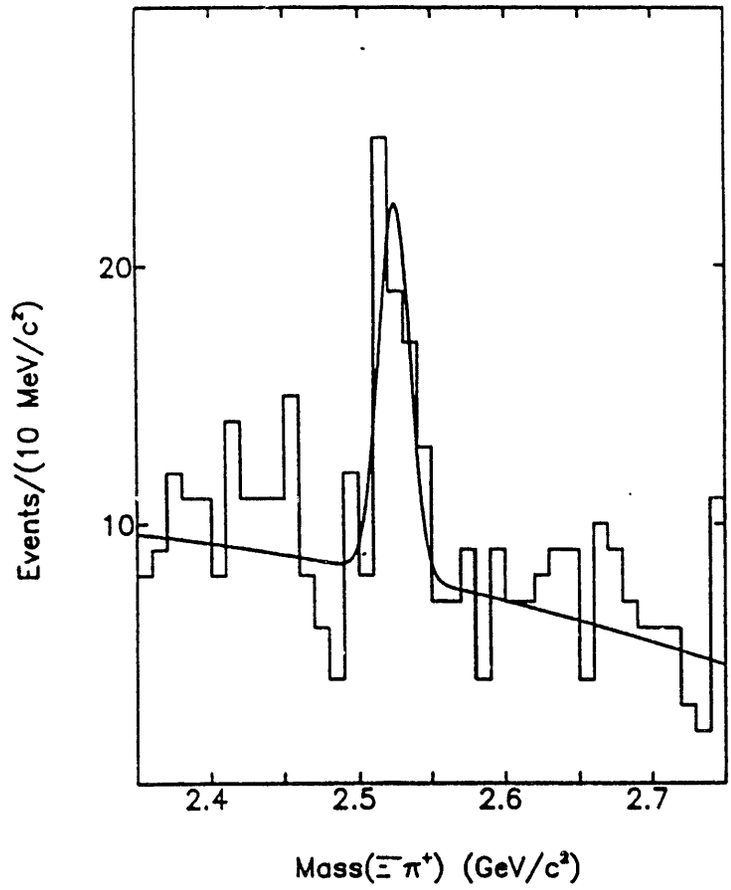

Figure 20: The $\Xi^-\pi^+$ mass distribution. The signal is fitted by gaussian with its width predicted by the Monte Carlo.

Ω^-'s. Other decays of $\Xi_c \to \Omega X$ are severly phase space limited, so probably do not contribute much.

ACKNOWLEDGEMENTS

I would like to thank the conference organizers for the invitation to speak at the conference. I would also like to thank my CLEO collegues who helped me prepare this report.

References

1. A. Chen *et al.* (CLEO), Phys. Rev. Lett. **51**, 634 (1983).

2. J.J. Hernandez *et al.*, Phys. Lett. **B239**, 1 (1990).

3. G. Fox and S. Wolfram, Phys. Rev. Lett. **41**, 1581 (1978).

4. G. Wormser *et al.* (Mark II), Phys. Rev. Lett. **61**, 1057, (1988).

5. For $\eta\pi^+$ J. C. Anjos *et al.* (E691), Phys. Lett. **B223**, 267 (1989); for $\eta'\pi^+$ J. C. Anjos *et al.* (E691), Phys.Rev. **D43**, 2063 (1991).

6. P. Kim (Mark III), "Results on Hadronic Decays of D and D_s Mesons from Mark III," in **Heavy Quark Physics**, ed. by P. Drell and D. Rubin, AIP (1989).

7. M.P. Alvarez *et al.* (NA14/2), Phys. Lett. **B255**, 639 (1991).

8. H. Albrecht *et al.* (ARGUS), Phys. Lett. **B245**, 315 (1990).

9. M. Bauer, B. Stech, and M. Wirbel, Z. Phys. **C34**, 103 (1987).

10. A. N. Kamal, N. Sinha, and R. Sinha, Phys. Rev. **D38**, 1612 (1988).

11. F. J. Gilman and R. Kaufmann, Phys. Rev. **D36** 2761 (1987).

12. B. Yu. Blok and M. A. Shifman, Sov. J. Nucl. Phys., **45** 522 (1987).

13. N. Isgur, D. Scora, B. Grinstein, and M. B. Wise, Phys. Rev. **D39**, 799 (1989)

14. M. Wirbel *et al.*, Z. Phys. **C29** (1985).

15. D. Scora, "D_s Semileptonic Decay in the Quark Model", submitted to PANIC conference, MIT, Cambridge, Massachusetts (1990).

16. J. Alexander *et al.* (CLEO), Phys. Rev. Lett. **65**, 1531 (1990)

17. R. J. Morrison *et al.* (CLEO), "Two-Body Decays to $\eta\pi^+$, $\eta'\pi^+$, $\eta\rho^+$, $\eta'\rho^+$, and $\phi\rho^+$ ", a paper submitted to the 1991 Photon-Lepton Conference, Geneva, Switzerland.

18. H. Albrecht *et al.* (ARGUS), Phys. Lett. **B255**, 634 (1991).

19. H. Albrecht *et al.* (ARGUS), DESY 90-157.

20. J. Adler *et al.* (MARK III), Phys. Lett. **B208**, 152 (1988).

21. L. Brekke and J. Rosner, Comments Nucl. Part. Phys. **18**, 83 (1988).

22. Kitagaki, T. *et al.*, Phys. Rev. Lett. **48**, 5 (1982).

23. Avery, P. *et al.*, Phys. Rev. **43**, 3599 (1991).

24. Kuar, G. and P. P. Khanna, Phys. ReV. **D44**, 182 (1991).

25. Avery, P. *et al.* (CLEO), Phys. Rev. Lett. **62**, 863 (1989).

26. Barlog, S. *et al.* (ACCMOR), Phys. Lett. **B236**, 495 (1990).

27. Albrecht, H. *et al.* (ARGUS), Phys. Lett. **B247**, 121 (1990).

28. Guberina, G. *et al.*, Z. Phys. **C33**, 297 (1986).

29. Basile, M. *et al.*, Nouvo Cimento **62**, 14 (1981)

30. Andrews, D. *et al.* (CLEO), NIM **211**, 47 (1983); Cassel, D. *et al.* (CLEO), NIM **A252**, 325 (1986) and Bebek, C. *et al.* (CLEO), Phys. Rev. Lett. **56**, 1893 (1986).

31. This is the same data sample that was presented in Alam, M. S. *et. al.* (CLEO), Phys. Lett. **B226**, 401 (1989) and in reference 25.

END

DATE FILMED

12/19/91